Inorganic Chemistry

Forum Article

pubs.acs.org/IC

Electronic Structure and Formation of Simple Ferryloxo Complexes: Mechanism of the Fenton Reaction

Alban S. Petit, Robert C. R. Pennifold, and Jeremy N. Harvey*

School of Chemistry and Centre for Computational Chemistry, University of Bristol, Cantock's Close, Bristol BS8 1TS, U.K.

Supporting Information

ABSTRACT: The Fenton reaction is a famous reaction in inorganic chemistry, with relevance to topics such as bioinorganic oxidation and fundamental redox chemistry of water and oxygen. It is also a reaction concerning which there has been very extensive mechanistic debate, with experimental and computational work leading to extensive evidence concerning its mechanism—not all of which is consistent. Here, we use this reaction as a challenge to modern electronic structure theory methods and show that density functional theory, when validated by accurate ab initio methods, can yield a picture of this reaction that is consistent with experiment. The article also highlights some of the challenges in accurate studies of reaction mechanisms of ionic species in water solution.

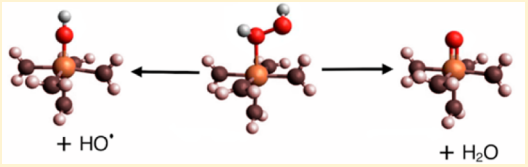

INTRODUCTION

Transition-metal oxo complexes $L_nM{=}O$ play central roles in the reaction mechanisms of many metalloenzymes and biomimetic oxidation catalysts, as well as in systems for water oxidation and reduction. Hence, gaining a good understanding of the structure and stability of these species, as well as of the mechanisms of the elementary reaction steps, leading to the formation and reaction of these species, is important for obtaining good control over these important processes. There has been considerable experimental and computational work aimed at characterizing the electronic and geometric structures of metal oxo complexes,and the reaction mechanisms involved in their formation and reaction.

In the gas phase, metal oxo ions MO^+ have been observed for a large number of both main-group and transition metals,[1,2] although this work focuses on the latter. The bond energies for many of these ions have been determined through a variety of mass spectrometric techniques.[1] For early transition metals such as scandium, titanium, or vanadium, the bond energy of these ions is very large because they adopt formal $M^{3+}{-}O^{2-}$ bonding patterns, with the electrons belonging to the $2p_z$ and $2p_x$ or $2p_y$ orbitals of the oxo dianion able to donate into empty d_{z^2} and d_{xz} or d_{yz} orbitals on the metal, thereby leading to a high triple bond order.[3] The remaining 0, 1, or 2 valence electrons on the metal can reside in formally nonbonding d_{xy} and/or $d_{x^2-y^2}$ orbitals of δ symmetry. For later transition metals, the increasing d electron count progressively leads to low bond orders as the antibonding orbitals are occupied,[2] with the CuO^+ bond energy being very weak.[4] Ions such as FeO^+ have an intermediate bond energy—high enough that they can be readily formed by oxidation of the bare metal ion through reaction with oxidants such as N_2O but small enough that they can transfer oxygen to reducing agents such as alkanes or hydrogen,[5,6] leading to the possibility of catalysis.[7] Another important trend across the periodic table is that, for later transition metals, the M−O bond becomes less polar as the metal atom's ionic radius decreases. Indeed, for FeO^+, which has a sextet ground state, the oxygen atom is best described as having oxyl character with one unpaired electron and a formal iron(II) metal center.[2] The electronic structure of the ground state of this metal oxo ion has been described as similar to that of the $^3\Sigma$ ground state of dioxygen (O_2), with two unpaired electrons sitting in π^* orbitals that are roughly evenly distributed between the metal and the oxygen.[2] There is a relatively low-lying quartet state, analogous to the $^1\Delta$ state of O_2, in which these π^* orbitals are paired up. As for O_2 also, the reactivity of the high-spin and low-spin states is rather different, with the sextet species typically undergoing hydrogen-atom abstraction to form $FeOH^+$ and the quartet species favoring formal insertion of the FeO moiety into covalent bonds.

These gas-phase trends for the bare metal ions are to some extent mirrored by the solution behavior of the corresponding transition-metal oxo species. Early transition metals form many stable oxo or polyoxo complexes, but as the d shell of the metal is progressively filled up, the prevalence and stability of these complexes decrease, until one hits an "oxo wall" between iron and cobalt, beyond which stable terminal metal oxo complexes are very much less likely to be observed.[8] Again, oxo complexes of metals such as iron represent a midpoint in that they are stable enough to be formed and characterized but reactive enough to participate in many oxidation processes[9] and are also commonly involved in bioinorganic chemistry.[10] For iron(IV) oxo species $LFeO^{2+}$, electronic structure and reactivity patterns similar to those mentioned above for the bare FeO^+ ion are found. For example, there are typically close-lying high-spin and

Special Issue: Insights into Spectroscopy and Reactivity from Electronic Structure Theory

Received: February 16, 2014
Published: May 1, 2014

   dx.doi.org/10.1021/ic500379r | Inorg. Chem. 2014, 53, 6473−6481

low-spin states, and the oxygen atom often has significant oxyl character and radical-like atom abstraction reactivity.[11]

The formation of metal oxo complexes can occur in a number of different ways. For the early transition metals with a tendency to form very stable oxo species, one important route to their formation is hydrolysis of species such as halides. Here we will, however, focus on oxidative processes $M(n) + XO \rightarrow M(n+2){=}O + X$, where XO is an oxygen donor such as ozone, peroxo acids (e.g., mCPBA), alkyl peroxides (tBuOOH), or hydrogen peroxide (H_2O_2). In bioinorganic chemistry, O_2 frequently serves as the oxidant species, leading to oxo formation, although here a coreducing agent R (such as NADPH) is usually involved, corresponding to the overall transformation $M(n) + O_2 + R \rightarrow M(n+2){=}O + RO$.[9] This usually involves more than one elementary reaction step, with the intermediacy of species in which the metal is bound to a O_2 moiety that has been partially reduced to the peroxo oxidation state, e.g., MOOH.[12]

O−O bond cleavage in peroxide species is thereby a rather common pathway for the formation of metal oxo complexes, and many experimental and computational studies have addressed the mechanisms of such processes. For iron complexes, rather different behavior is found depending on the ligands, the conditions, and the initial oxidation state of the metal. As discussed in an excellent review,[13] iron(III) hydroperoxo complexes can undergo very different decomposition routes (Scheme 1), depending on the nature of the

Scheme 1

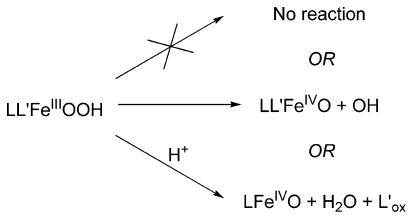

partner ligands (and on the presence or not of vacant sites at the metal). In some cases, the hydroperoxo species are rather stable, while in others, iron(IV) oxo species are formed by homolysis of the O−O bond, and in still others, a reaction with acid occurs, leading to heterolysis and oxidation of a coligand (e.g., carboxylate, which is then lost as $RCO_2^{\bullet}$).

This last possibility is related to a key step in the catalytic cycle of the cytochrome P450 enzymes.[14] A ferric heme group undergoes successive one-electron reduction, O_2 binding, one-electron reduction, and protonation to yield a heme-OOH (sometimes referred to as compound 0). This then undergoes proton-assisted O−O bond heterolysis to yield water and an iron oxo species, known as compound I, in which iron is formally in the V+ oxidation state. However, both electronic structure studies[15] and experiment[16] show that, in fact, the iron is in the IV+ oxidation state and the heme group has undergone one-electron oxidation. Unlike the case shown in Scheme 1, this does not lead to ligand loss, but instead the heme group has a "hole" in the π system. The breaking of O−O bonds in peroxide metal complexes are also important mechanistic steps because they are the reverse of steps in the heavily investigated water oxidation reactions.[17,18]

One of the most important elementary reactions that has been suggested to lead to the formation of a metal oxo complex is the Fenton reaction of aqueous ferrous ions with hydrogen peroxide.[19] Some experimental evidence suggests that this reaction leads to formation of the iron(IV) species FeO^{2+} (the parent ferryl ion) through formal oxygen-atom transfer. Indeed, in a related reactivity of ferrous complexes with more complex ligands, as was already mentioned, oxo formation is well established and finds synthetic utility. However, the most careful experimental studies conclusively show that, at the low pH values typically used for the Fenton reaction, no ferryl ions are formed.[20] Hydroxyl radicals and ferric ions are produced instead, arising from homolysis of the O−O bond in iron-coordinating hydrogen peroxide. In contrast, the use of other oxidants, e.g., ozone, does convert ferrous ions into ferryl ions, and these can be characterized in aqueous conditions, clearly showing that they are stable in water.[17] Also, at higher pH values, the evidence suggests that the homolysis pathway, leading to a hydroxyl radical, and the oxygen-transfer pathway, leading to ferryl ions, become competitive.[21] Clearly, the reaction pathways leading to homolysis and heterolysis of the O−O bond must lie close in energy.

The motivation for the present Forum Article is the fact that previous computational work using density functional theory (DFT) has suggested that oxo formation should dominate in the parent Fenton reaction.[22,23] This conclusion is not consistent with the most recent careful experimental observations at low pH.[17] This fairly stark discrepancy between experiment and computation concerning the chemistry of the most simple iron oxo species is puzzling and a challenge, given the extensive computational work carried out relating to the electronic structure and reactivity of other metal oxo species.

In principle, this disagreement could be explained in a number of ways. These possibilities are fairly generic when confronting experimental and computational results that are apparently inconsistent, making the present problem into an excellent exemplar for discussing the strategy to be adopted in such cases. First, the experimental results could, in principle, be incorrect, or there could be some confounding element in the way the experiments were designed such that their results could have been interpreted incorrectly. Clearly, this does happen, and computational chemists can play an important role in such cases by maintaining a dialogue with experimental colleagues. In fact, we have often found that one of the more useful contributions we can make in collaborations is to identify interpretations of experimental results that *cannot* be correct. For example, in a recent study of alkene cis−trans isomerization catalyzed by palladium(II), a key contribution made very early in our computational work was the prediction that C−C bond rotation in a species in which the alkene was coordinated to palladium simply could not occur with a barrier low enough to be consistent with experimentally observed rates.[24] When the initially proposed mechanism was confidently ruled out, it was possible to help the experimental colleagues explore alternative routes and ultimately find a mechanism that was consistent with detailed kinetic results and computation.

A second possibility is that the electronic structure method used is not accurate enough and incorrectly favors one route over another. Given the typical magnitude of the errors that are known to occur in DFT studies of transition-metal compounds,[25] this possibility should always be taken seriously. In fact, we will argue below that this is the main reason for the discrepancy in the case of the Fenton reaction. It should, however, be noted that, in many other cases, predictions concerning which of several mechanisms is favored can be more robust than one might expect given the known accuracy of

dx.doi.org/10.1021/ic500379r | Inorg. Chem. 2014, 53, 6473−6481

electronic structure methods. This is because it is quite often the case that the critical points along competing reaction profiles share many features in terms of the electronic structure, such that favorable error cancellation is expected. DFT as well as other electronic structure methods tends to yield quite accurate relative energies when the species being compared share many bonding features. This explains the success of rather inaccurate methods such as Hartree−Fock theory for predicting relative energies of species containing the same number of each type of chemical bond (isodesmic reactions).[26]

A third possibility is that other aspects of the theoretical treatment are inaccurate. For example, competing pathways might differ considerably in terms of their entropic properties, their solvation properties, and/or their ability to be described using a given microscopic model system. Reactivity depends on free energy, not potential energy, and entropy effects can make a major contribution to free energy. This is particularly so for reactions in which the number of independent molecular entities changes between the reactant state and the rate-limiting transition state (TS). There has been some debate about the correct way to include entropic effects for reactions in solution, with different approaches[27,28] leading to differences in the free energies of activation that can easily be of 5 kcal mol^{-1} or more. Solvation effects can also lead to large changes in free energy, especially in a comparison of states with a very different distribution of charge, so aqueous reactions of ions, such as the Fenton reaction, are potentially particularly challenging. Finally, any computational model of a chemical reaction requires the selection of a microscopic model, a set of atoms whose motions are needed to describe the elementary reaction steps that are assumed to occur. The effect of other atoms—such as those of the solvent—can be treated at least approximately through the use of a continuum solvent model. However, if the correct mechanism involves a step such as solvent participation that cannot, in principle, be described by the microscopic model used, then errors will result.

In this study, we use new DFT calculations, as well as accurate wave-function-based electronic structure theory, to study the thermodynamics and kinetics of the competing pathways in the Fenton reaction. The key here is the use of a new explicitly correlated version of coupled-cluster theory [CCSD(T)-F12[29]], which enables us to obtain accurate energies despite using a fairly modest-sized basis set. By doing this and paying attention to the other aspects just mentioned, we obtain a good model of the reaction at low pH. This enables us to show that ferryl ion production is indeed not as facile as was found in the earlier computational work. We further show that the energy barriers leading to ferryl ion formation and O−O bond homolysis are similar and that the presence of electron-donating ligands on the metal center favors formation of the ferryl ion. Hence, the discrepancy with experiment is removed. In light of these results, we will also revisit some of the challenges just mentioned that are involved in the quantitative description of metal-ion redox chemistry in aqueous solution and propose solutions.

■ COMPUTATIONAL DETAILS

The structures of all species were initially optimized using the B3LYP functional, including the −D2 dispersion correction of Grimme,[30] with the all-electron 6-311G(d) basis set for iron and the 6-31G(d) basis set for other atoms. Open-shell species were treated using an unrestricted orbital approach. At the stationary points, second derivatives were computed in order to check that minima or TSs were obtained. Great care was needed in order to find true minima for some of these systems because they typically have low-symmetry structures using the present cluster model, although they are very close to adopting the symmetry of higher-order point groups. For example, the $Fe(OH_2)_6^{2+}$ species is relatively close to adopting a high-symmetry equilibrium structure belonging to the T_h point group. However, a number of factors lead to distortion away from this symmetric structure, such that the global minima are found to correspond to much less highly symmetric point groups, typically C_1 for most of the species covered here.

Considering the example of the ferrous ion in detail to illustrate this point, the Jahn−Teller effect obviously leads to symmetry breaking in the $Fe(OH_2)_6^{2+}$ model that we use for the aqueous ferrous ion (which is $t_{2g}^4e_g^2$ in its ground quintet electronic state). This leads to small differences between the Fe−O bond lengths, as noted in a previous study.[31] Other less obvious factors also lead to further symmetry breaking, e.g., weak hydrogen bonding between the water molecule ligands, and secondary bonding interactions between the π-symmetric lone pairs on the water molecules and the metal d orbitals. These lead to effects such as slight rotations of the water ligands around the Fe−O axes.[32] As a result of these effects, the global minimum of the $Fe(OH_2)_6^{2+}$ species is found to belong to the C_1 point group. All symmetric structures, even those with only low symmetry, e.g., C_s or C_2, are found to lie higher in energy and yield one or more imaginary vibrational frequencies. However, the energy difference between the nonsymmetric minimum and structures with slightly higher symmetry is small. For example, the C_1 minimum lies only 0.3 kcal mol^{-1} below the lowest point with D_{2h} symmetry; note that this latter point group allows for Jahn−Teller distortion. Similar very small distortions are found for other species. While it is likely that the extent and nature of symmetry breaking is dependent on the level of theory used, test calculations confirm that highly symmetric structures have one or more imaginary frequencies using a variety of DFT functionals and basis sets.

The vibrational frequencies and rotational constants for the optimized structures were used to compute zero-point energy and thermal corrections, using the rigid-rotor, harmonic oscillator approximation. The program's default standard state corresponding to an ideal gas at a standard pressure of 1 atm was changed to use either a standard state of 1 M (most species) or of 55.5 M (for water molecules). These calculations were all performed in a vacuum. The vacuum energies were corrected by including a single-point estimate of the free energy of solvation in water, calculated using the SMD model,[33] using the B3LYP level of theory and the same basis set. All of these DFT calculations were performed using the *Gaussian 09* program package.[34]

Single-point energies were also obtained using DFT and correlated ab initio methods, using the *MOLPRO* program package.[35] The DFT calculations were performed with the B3LYP and BP86 functionals, as implemented in *MOLPRO*. Coupled-cluster theory calculations were performed with partial spin restriction in the excitation amplitude, and in all cases, the semicore 3s and 3p electrons on iron were included in the correlation treatment. As well as standard CCSD(T) calculations, near-basis-set limit results were obtained by performing CCSD(T) calculations with explicit treatment of electron−electron correlation (F12b approach[26]). The occurrence of near-degeneracy effects was tested by computing the t_1 diagnostic and inspecting large single- and double-excitation amplitudes. The t_1 diagnostic was on the order of 0.01 for the iron(II) species, 0.03 for iron(III), and 0.05 for iron(IV). There are single-excitation amplitudes that are up to 0.30 and doubles up to 0.12. At first sight, this indicates some multireference character, and the accuracy of the coupled-cluster calculations could therefore be questioned. However, as in previous work,[6] we found that test coupled-cluster calculations using Kohn−Sham orbitals to expand the wave function returned very similar total energies but with much smaller t_1 diagnostic values and single-excitation amplitudes. Explicit treatment of electron−electron correlation is not currently possible in such Kohn−Sham coupled-cluster calculations, so these have only been performed as tests of the accuracy of the coupled-cluster method but are not reported.

dx.doi.org/10.1021/ic500379r | Inorg. Chem. 2014, 53, 6473−6481

To treat relativistic effects, the Douglas–Kroll operator to second-order was used in some cases. The use of this operator is currently not possible using explicit correlation, so relativistic CCSD(T)-F12 energies were approximated as E[CCSD(T)-F12-DK] ≈ E[CCSD-(T)-F12] + E[CCSD(T)-DK] − E[CCSD(T)]. In these calculations, the iron atom was described using the cc-pwCVTZ basis set,[36] while the oxygen and hydrogen atoms were treated using either the cc-pVTZ or cc-pVDZ basis set. Where the Douglas–Kroll Hamiltonian was used, adapted forms of these basis sets (e.g., cc-pwCVTZ-DK for iron) were used. Where needed, appropriate auxiliary basis sets were used in order to enable density fitting or related approximations (a sample input file showing the combination used is included in the Supporting Information, SI).

Correlated calculations are much more efficient when molecular symmetry is present. In our calculations, we have carried out the CCSD(T) single-point calculations at structures more highly symmetric than the global DFT minimum wherever the DFT method returns a more symmetric structure that lies less than 0.3 kcal mol^{-1} higher in energy than the global minimum. Because this energy difference is much smaller than other sources of error, the estimated free energy at the CCSD(T) level (G_{CC}) has been obtained by the approximate expression $G_{CC} \approx G_{DFT} - E_{DFT} + E_{CCSD(T)}$, where the DFT values are obtained at the lower-symmetry minimum-energy structures, and the coupled-cluster values are obtained at the close-lying, more symmetric structures. A full list of the less and more symmetric structures used, with their point groups, is included in the SI.

RESULTS

We start by considering the reaction of $Fe(OH_2)_6^{2+}$ with H_2O_2, leading to competing formation of the ferryloxo species $(H_2O)_5FeO^{2+}$ or the ferric species $(H_2O)_5FeOH^{2+}$ and hydroxyl radical. Near pH = 1, where the recent experimental work on the Fenton reaction was performed,[17] the formulas given here correspond to the preferred charge state of the iron center, and this is how the species have been modeled in the calculations.

The structures of the various species involved in the oxidation of Fe^{2+}_{aq} by H_2O_2, for the present cluster model described at the B3LYP-D2 level of theory, are rather similar to those obtained in previous studies using other DFT and related methods[20] and hence will not be extensively discussed here. All optimized structures are included in the SI. We have calculated solution-phase free energies using a composite method based on computing gas-phase free energies at the B3LYP-D2 level and adding corrections based on a much more accurate electronic structure method (CCSD(T)-F12) and on a continuum model of solvation free energy to describe the aqueous environment.

The mechanisms leading to competing formation of the iron(IV) oxo and iron(III) hydroxo complexes and $^{\bullet}OH$ radical are shown in Scheme 2. First, H_2O_2 enters the iron coordination sphere. We treated this as a dissociative substitution through a pentacoordinate $Fe(OH_2)_5^{2+}$ species. Experiment suggests that water exchange at an aqueous ferrous ion occurs through an I_D mechanism,[37] involving the synchronous departure of one ligating group and arrival of another, with dissociative character dominating. This is likely true for the present exchange also. The rate constant for water exchange is on the order of 4×10^6 s^{-1}. For water at ca. 55 M, this is equivalent to a bimolecular rate constant of ca. 10^5 M^{-1} s^{-1}. Assuming that a similar rate constant is obtained for substitution with an incoming H_2O_2 molecule, then clearly this exchange step cannot be rate-determining, given the experimentally measured value of ca. 50 M^{-1} s^{-1}. Hence, we did not seek to model the exchange more accurately.

Next, homolysis of the O–O bond can lead to ferric $(H_2O)_5Fe(OH)^{2+}$ and hydroxyl radical, through TS 1 in Scheme 2. We find that, upon stretching of the O–O bond, the energy smoothly increases as the structure and electronic structure of the species change toward that of the products, and we therefore assume that the reverse of this reaction (the addition of a hydroxyl radical to ferric hydroxide to form a hydrogen peroxide complex) occurs without a potential energy barrier. In solution, the rate constant for the hypothetical reverse reaction would be determined by diffusion of the two species toward one another, and hence the rate constant would be on the order of 10^{10} M^{-1} s^{-1}. By inverting the Eyring equation, this is equivalent to an activation free energy of 3.8 kcal mol^{-1}. Adding this to the computed equilibrium free-energy change for the forward reaction provides us with a computational rough estimate of the free energy of the barrier TS 1 to this homolytic reaction step.

In competition with this step, O–O cleavage can occur heterolytically to yield an iron(IV) species. As in the previous work by other authors,[20] we found that the lowest-energy pathway leading to such cleavage occurs through a hydrogen atom (or proton) shuffle pathway, as shown, leading initially via TS 2 to an iron(IV) dihydroxide species. We have modeled this both as $(H_2O)_4Fe(OH)_2^{2+}$ and as $(H_2O)_4Fe(OH)_2^{2+}\cdot H_2O$, a complex in which the departing second hydration sphere water molecule is explicitly modeled. As discussed further below, it is pleasing to note that these two microscopic models yield very similar calculated free energies, suggesting that our computational protocol is able to describe free energies in solution accurately.

The dihydroxoiron(IV) complex can undergo intramolecular proton shuffling to form the more stable ferryloxo species through TS 3. This can occur by direct proton transfer from one OH group to the other, but this involves a fairly strained arrangement, formally a four-membered ring. As in previous work,[20] we find that indirect proton transfer with participation of a second-sphere water molecule leads to a lower free-energy barrier.

The free energies calculated for the various species in Scheme 2 are shown in Table 1 and Figure 1. Results are shown with our preferred method, B3LYP, including a correction for dispersion, and we will focus on these results initially. However, we also include relative free energies computed using the BP86 functional, for consistency with previous work.[20] These will be discussed below. The first step, dissociation of water from a hexacoordinate ferrous ion, is predicted by the calculations to be *favorable* with both functionals. Taken at face value, this would suggest that iron prefers to be pentacoordinate. However, the present calculated free energies include a

Scheme 2

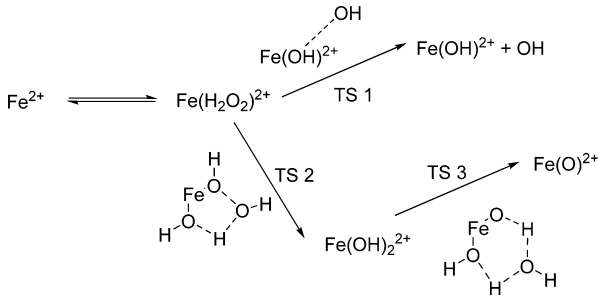

dx.doi.org/10.1021/ic500379r | Inorg. Chem. 2014, 53, 6473–6481

Table 1. Calculated Relative Free Energies (kcal mol^{-1} at 298 K) in Aqueous Solution, Where Additional Water Molecules Are Included As Needed

species	$\Delta G(\mathrm{BP86})_{aq}$	$\Delta G(\mathrm{B3LYP\text{-}D2})_{aq}$
$Fe^{II}(OH_2)_6^{2+} + H_2O_2$	0.0	0.0
$Fe^{II}(OH_2)_5^{2+} + H_2O_2$	−6.5	−5.2
$Fe^{II}(OH_2)_5(H_2O_2)^{2+}$	4.6	5.5
TS 1	6.4[a]	11.1[a]
$Fe^{III}(OH_2)_5(OH)^{2+} + OH$	2.6	7.3
TS 2	−0.8	13.0
$Fe^{IV}(OH_2)_4(OH)_2^{2+}$	−31.1	−2.3
$Fe^{IV}(OH_2)_4(OH)_2^{2+}\cdot H_2O$	−32.8	−1.5
TS 3[b]	−31.2	0.3
$^5Fe^{IV}(OH_2)_5(O)^{2+}\cdot H_2O$	−33.8	−7.7
$^5Fe^{IV}(OH_2)_5(O)^{2+}$	−33.7	−8.4

[a]This value is obtained by making the assumption that the rate for the hypothetical reverse reaction would be diffusion-limited, with a rate constant at room temperature of 10^{10} M^{-1} s^{-1}. [b]The calculated relative free energies for this TS in the absence of a second-hydration-sphere water molecule are respectively −15.8 and +15.8 kcal mol^{-1} at the BP86 and B3LYP-D2 levels of theory.

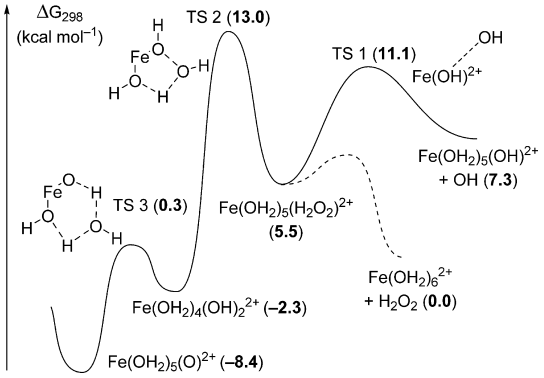

Figure 1. Calculated B3LYP-D2 free-energy surface (at 298 K) for the Fenton reaction.

contribution from the SMD continuum solvent model. This will depend on the interactions between the solute and continuum solvent on the exposed surface area of the solute. Because the pentacoordinate iron has a square-based-pyramidal structure, the iron is solvent-exposed, and hence the continuum model will include a free-energy contribution arising from "solvation" of the metal. This means that the calculation effectively describes a fully solvated ferrous ion, and the free-energy difference would be zero here if the continuum model could account exactly for metal−water interaction.

The second step involves the coordination of H_2O_2 and is favorable in free-energy terms, although the resulting hydrogen peroxide complex is predicted to be *less* stable than the starting species. This suggests that H_2O_2 acts as a poorer ligand to iron than does water. Other computational studies of water−hydrogen peroxide exchange on metal centers[38] have found that this step is endothermic. Note that, in the present case, the choice of a standard state for H_2O (55.5 M) and H_2O_2 (1 M) accounts in large part for the unfavorable standard free energy of substitution.

As was already mentioned, homolysis of the O−O bond leads without a potential energy barrier to iron(III) hydroxide and a hydroxyl radical. The electronic structure varies smoothly from the starting species, with four unpaired electrons on the high-spin d^6 iron, to the products, with high-spin d^5. Within the unrestricted Kohn−Sham DFT approach used here, the developing unpaired electron density on the hydroxyl radical is "spin-down", thereby yielding a net $S_z = 2$ state. In order to calculate the rate constant for homolysis, we need to know the free energy of the corresponding TS. Because there is no saddle point on the potential energy surface for this step, the free energy for the TS cannot be computed in the standard way using statistical mechanics at the TS structure. Instead, the free energy of activation for this step is estimated as mentioned above, based on the assumption that the putative recombination of OH with the ferric hydroxide would be diffusion-limited. This yields a free energy that is just 5.6 kcal mol^{-1} above the hydrogen peroxide complex, corresponding to a very small free-energy barrier to O−O bond breaking. Assuming that this step is rate-limiting in the reaction of hydrogen peroxide with a ferrous ion, the free energy of activation would be 11.1 kcal mol^{-1}. Using the Eyring equation, this translates to a predicted rate constant of 4×10^4 M^{-1} s^{-1} for the initial step in the Fenton reaction of a ferrous ion. The experimental value is 5.8×10^1 M^{-1} s^{-1},[19] roughly 700 times smaller. This equates to an error in the predicted free energy of 3.9 kcal mol^{-1}, which, considering the uncertainties in the DFT method and continuum solvent model, is not unreasonable.

The barrier to the competing process, formation of iron(IV), is higher, at 13.0 kcal mol^{-1}. As was already discussed, this agrees with the experimental observation whereby the reaction with H_2O_2 does not lead to the ferryl ion but does lead to chemistry consistent with OH formation. The difference in the barrier heights, of 1.9 kcal mol^{-1}, is equivalent to a reactivity ratio of 25. Experiment clearly concludes that the ferryl ion cannot be produced in large amounts from the reaction of H_2O_2 with a ferrous ion at low pH. It is less easy to deduce what is the maximum amount of the ferryl ion that could be produced as a minor product, but we assume that this is on the order of 1%, and our calculated difference in the barrier height is thereby at least qualitatively consistent with experiment. As was already mentioned, the present free energies have some uncertainties mainly because of the DFT functional and continuum solvent model.

If formed, the dihydroxoiron(IV) complex would readily convert to the ferryl ion, over the proton shuttle TS 3. In order to bring this TS onto the same free-energy surface as the starting species, we need to include an additional water molecule in the model. If the continuum model performs correctly, the calculated free-energy difference between $(H_2O)_4Fe(OH)_2^{2+} + H_2O$ and the species with one water in the second hydration sphere, $(H_2O)_4Fe(OH)_2^{2+}\cdot H_2O$, would be equal to zero because these are effectively the same species. As can be seen in Table 1, the calculated free-energy difference is indeed very small, at just 0.8 kcal mol^{-1}. The barrier to the proton-shuttled rearrangement is then very small, just 1.8 kcal mol^{-1}, and leads to the more stable oxo form, also with a water molecule in the second hydration sphere of $(H_2O)_5FeO^{2+}$. This too is very close in calculated free energy to the corresponding separated $(H_2O)_5FeO^{2+}$ and water, showing that the continuum solvent model performs well in this respect. The greater stability of the oxo form of the iron(IV) ion is consistent with the fact that when generated by oxidizing the ferrous ion with isotopically labeled ozone, the label is not found to scramble onto the other oxygen atoms.

Turning to the comparison between the B3LYP-D2 and BP86 results in Table 1, it can be seen that these methods agree

dx.doi.org/10.1021/ic500379r | Inorg. Chem. 2014, 53, 6473−6481

Table 2. Calculated Relative Energies (kcal mol^{-1}, in the Gas Phase unless Mentioned Otherwise)

species[a]	BP86	B3LYP	B3LYP-D2	B3LYP-D2[b]	CCSD(T)[c]	CCSD(T)
$Fe^{II}(OH_2)_6^{2+} + H_2O_2$	0.0	0.0	0.0	0.0	0.0	0.0
$Fe^{II}(OH_2)_5^{2+} + H_2O_2$	24.0	25.3	28.4	2.6	27.5	27.3
$Fe^{II}(OH_2)_5(H_2O_2)^{2+}$	2.0	2.9	2.0	0.1	−0.8[d]	−0.9[d]
$Fe^{III}(OH_2)_5(OH)^{2+} + OH$	18.7	23.4	23.3	8.6	27.9	23.9
$Fe^{IV}(OH_2)_4(OH)_2^{2+}$	−6.4	22.3	22.7	−3.0	38.4	31.8
$^5Fe^{IV}(OH_2)_5(O)^{2+}$	−8.0	17.2	17.5	−9.8	25.3	20.9

[a]Additional water molecules are present as required. [b]The results in this column include the approximate solvation free energy, derived from the continuum model. [c]These values are calculated *without* treatment of relativistic effects. [d]For this species, the CCSD(T)-F12 calculation was performed with a smaller basis set.

reasonably well on some aspects, e.g., the energy for the water−hydrogen peroxide exchange process. BP86 predicts that the ferric hydroxide product can be formed at slightly lower energy than B3LYP-D2. The big difference, though, lies in the relative free energy of the iron(IV) species, which are predicted to be far more stable in relative terms with BP86. Because the BP86 energy of TS 2 is evaluated as a single-point calculation at the B3LYP structure, the much greater exothermicity leads to the calculated energy of this TS lying *below* the energy of the preceding minimum. Although this energy would certainly increase if the TS structure was optimized at the same level of theory, there is little doubt that, at the BP86 level, the route to iron(IV) over TS 2 and TS 3 is favored over that leading to iron(III) and the $^{\bullet}$OH radical over TS 1. This is consistent with previous computational work[20,21] using the BP86 functional or related gradient-corrected functionals, in which ferryl ion formation was predicted to be facile.

Different DFT methods are well-known to yield rather different calculated relative energies for systems containing transition-metal compounds. It can be difficult to decide which functional gives the correct answer in such cases. Indeed, in the present case, the BP86 functional appears to predict incorrectly that iron(IV) formation should predominate in the Fenton reaction. However, this discrepancy between the BP86 predictions and experiment could arise for a number of reasons such as the use of an inappropriate microscopic model or the existence of other, nonmodeled reaction pathways. Also, the fact that the B3LYP calculations lead to qualitative agreement with experiment could be accidental. To resolve these issues, we recalculated the energy of the key species in Table 1 using a variety of methods, including the highly accurate CCSD(T) approach, which provides a benchmark. The results, given as zero-point energy-corrected electronic energies, are shown in Table 2.

It can be seen from Table 2 that many aspects of the theoretical model have quite large effects on the calculated relative energies. Columns 1 and 3 mirror the values in Table 1, except that here nonrelativistic electronic energies in the gas phase rather than solution-phase free energies are shown. Loss of a $^{\bullet}$OH radical from the hydrogen peroxide complex is now more endothermic. In contrast, water loss to yield the iron(IV) species remains highly favorable in the BP86 calculations but is quite endothermic with B3LYP. Columns 2 and 3 show the effect of dispersion corrections. While these are increasingly recognized to play an important role in transition-metal chemistry,[39] in the present case, the effect is relatively small, with only the dissociation energy from hexacoordinate iron hexaaqua to the pentacoordinate species being noticeably affected. Dissociation is, of course, particularly sensitive to errors in the treatment of dispersion.

Columns 3 and 4 illustrate the strong solvation effects in this system. All of the points on the potential energy surface include one doubly charged cation and neutral molecules. Hence, to a first approximation, one might expect that solvation effects would not be too strong. As was already discussed above in the context of Table 1, the continuum model does lead to a large stabilization of the pentacoordinate species, but this is in some sense an artifact whereby the continuum model is, approximately, describing water interaction with the sixth coordination site. More striking is the fact that there is a clear correlation between the metal's formal oxidation state and stabilization by the solvent field. Iron(III) hydroxide is lower in energy by ca. 15 kcal mol^{-1} in the presence of the continuum, and iron(IV) dihydroxide and the oxo species are lowered by ca. 25 kcal mol^{-1}. This reflects the fact that the higher formal charge on the metal polarizes the coordinated water molecules to a greater extent, and they therefore expose more positively charged protons to the continuum and interact more strongly with it. In the real system, this would correspond to enhanced hydrogen bonding to the second (and subsequent) hydration spheres around the metal.

Columns 5 and 6 contain the results from the ab initio benchmark. This uses the CCSD(T) method, with explicit treatment of correlation (the f12 method[27]). The applicability and accuracy of this single-reference method needs to be discussed first. We have found that CCSD(T) yields a reasonable description of many transition-metal compounds,[40] even where significant evidence of partial multireference character is found. Here, the t_1 diagnostic is large (0.05) for the iron(IV) species, and large single amplitudes are found. Test CCSD(T) calculations with Kohn−Sham orbitals, however, return almost identical total energies and yield t_1 diagnostics that are near zero, indicating that the large single amplitudes in the standard CCSD(T) calculations reflect the poor quality of the Hartree−Fock reference rather than intrinsic multireference character. This all mirrors almost exactly the observations made for the bare FeO^+ cation,[6] where additional calculations confirmed the accuracy of the CCSD(T) energies.

Focusing next on the difference between the relativistic and nonrelativistic columns, like the other values in the table, column 5 does not account for relativistic effects, whereas column 6 does, by using one-electron integrals calculated using the Douglas−Kroll Hamiltonian to second order. Here again, the main effect is on the relative energy of a species with a different formal oxidation state, with iron(III) and especially iron(IV) more highly favored when the relativity is taken into account. This is readily understandable because oxidation formally occurs from the metal's d orbitals, and the net effect of the relativity is to destabilize these orbitals.[41] Next, it is

dx.doi.org/10.1021/ic500379r | Inorg. Chem. 2014, 53, 6473−6481

instructive to compare column 6 with the energies obtained with the various DFT methods. Clearly, none of these agree perfectly with CCSD(T). The BP86 method predicts the iron(IV) species to be much more stable than the benchmark CCSD(T) calculations do. Even the B3LYP method slightly overestimates their stability, especially for the dihydroxy species. For the pathway leading to iron(III) and a hydroxyl radical, both BP86 and especially B3LYP are in good agreement with the benchmark.

The conclusion from this calculation is that the B3LYP-D2 results in Table 1 are much more reliable than those obtained with BP86. Hence, the fair agreement between the B3LYP-derived free energies and the experimental observations appears to be obtained "for the right reason". In fact, given that B3LYP slightly overestimates the stability of the iron(IV) dihydroxo species, it most likely also somewhat overestimates the stability of the TS leading to this species (TS 2). Hence, the small 1.9 kcal mol^{-1} gap between the predicted barriers for the experimentally observed pathway and the potential side reaction is probably too small. Unfortunately, this TS is not accessible to CCSD(T) calculations because of its size, symmetry, and multireference character.

In Table 3, we have computed the relative free energies for the key species in pathways leading to iron(III)- or iron(IV)-oxidized intermediates in reactions of modified iron(II) ions. First, we consider the deprotonated iron(II) species $(H_2O)_5FeOH^+$ as a model for Fenton chemistry at higher pH.[19] Next, we consider the chemistry of the ammonia analogue $Fe(NH_3)_6^{2+}$. This is a model for the chemistry of iron(II) complexes with polyamine ligands.[9,13] In this system, the triplet state of the iron(IV) oxo species was found to be lower in energy than the quintet state. Coupled-cluster calculations are not reported for the ammonia analogues here, partly because the species involved are larger and do not even approach the higher symmetries needed for efficient coupled-cluster calculations. Also, some of the ammonia-containing species led to poor behavior of the coupled-cluster expansion, presumably because of the multireference character of the wave function.

Table 3. B3LYP-D2 Relative Free Energies (kcal mol^{-1} at 298 K) in Aqueous Solution[a]

species	ΔG_{aq}	species	ΔG_{aq}
$(H_2O)_5Fe^{II}(OH)^+ \cdot H_2O + H_2O_2$	0.0	$^5Fe^{II}(NH_3)_6^{2+} + H_2O_2$	0.0
$(H_2O)_4Fe^{II}(OH)(H_2O_2)^+$	*b*	$^5Fe^{II}(NH_3)_5(H_2O_2)^{2+} + NH_3$	8.1
$(H_2O)_4Fe^{III}(OH)_2^+ + OH$	−8.1	$^6Fe^{III}(NH_3)_5(OH)^{2+} + OH + NH_3$	11.2
$^5Fe^{IV}(OH_2)_4(OH)(O)^+$	−25.0	$^3Fe^{IV}(NH_3)_5(O)^{2+} + NH_3$	−21.9

[a]Additional water molecules are present as required. [b]This species was not included in the study.

The structure obtained for the deprotonated iron(II) species $(H_2O)_5Fe(OH)^+$ was rather distorted because of formation of a strong hydrogen bond between the hydroxide ligand and a neighboring water molecule. We considered that this structure was not realistic for describing the species in aqueous solution, so we instead described this system by adding one second-sphere water molecule that interacts with the hydroxide group, yielding a much more reasonable structure. The free-energy change for removing a proton from $Fe(OH_2)_6^{2+}$ to yield this ion is calculated to be 271.1 kcal mol^{-1}. Using the absolute free energy of the aqueous proton,[42] −263.1 kcal mol^{-1}, then yields a standard free energy for hydrolysis of a ferrous ion of 8.0 kcal mol^{-1}, or a calculated pK_a of 5.9, in fair albeit not excellent agreement with the experimental value[8] of 9.5. Note that quantitative calculation of the pK_a values still poses a considerable challenge to electronic structure theory combined with continuum models.[43]

Considering the values in Table 3, it can be seen that, in both cases, formation of the iron(IV) species is considerably more favorable than in the case of the aqua species in Table 1. As shown in Table 1, relative to the iron hexaqua ion, the initially formed dihydroxoiron(IV) species lies at −2.3 kcal mol^{-1}, and the oxo complex lies at −8.4 kcal mol^{-1}. Here, with the deprotonated iron complex, the iron(IV) oxo species lies at −25 kcal mol^{-1}, presumably because of stabilization of the more oxidized metal center by the more electron-donating hydroxo ligand. The iron(III) species is also stabilized but to a lesser extent (−8.1 vs 7.3 kcal mol^{-1} for the protonated case, as shown in Table 1). Note that these changes in the relative energy between iron(II), iron(III), and iron(IV) species as a function of the formal charge imply that the iron(III) and iron(IV) species are more acidic than the iron(II) ion. Indeed, the free-energy difference between $(H_2O)_5FeO^{2+}$ and $(H_2O)_4Fe(OH)(O)^+$ calculated here suggests a pK_a of −6.2. The experimental observation is, however, that, at a pH of ca. 1, the ferryl ion is doubly positively charged, so for ferrous ion, the pK_a value implied by our calculations is probably not highly accurate.

The main conclusion to be drawn from Table 3, though, is that a more electron-donating ligand environment makes the formation of iron(IV) from iron(II) and hydrogen peroxide more favorable in free-energy terms, with respect to both the starting iron(II) species and the alternative homolytic formation of iron(III) and a $^{\bullet}OH$ radical. The same trend is found for the oxo complex derived from the ammonia complex. This species has a triplet ground state, unlike the high-spin ground states found for all other species in this study. The higher stability of the ferryl ions in these last two cases agrees with the experimental observation[8] that ferryl species are much more readily formed in those cases.

■ CONCLUSIONS AND PERSPECTIVE

In this paper, we revisit the potential energy surface for the parent Fenton reaction between aqueous ferrous ion and hydrogen peroxide. We focus mostly on the chemistry at low pH and show that the free-energy barrier for forming a hydroxyl radical and iron(III) is lower than that for forming iron(IV) species. This is consistent with experiment[8] but not with previous calculations that predict that iron(IV) formation should dominate.

The difference between our results and previous calculations lies in the DFT functional used: B3LYP vs BP86 or PBE. These functionals yield *very* different relative energies for the iron(III) and iron(IV) species, with the difference much larger than the average error of both types of functional. This is presumably due to an important role for nondynamic correlation in the electronic structure of these metal complexes, presumably because of the challenging π bonding between iron and the oxo ligand. The BP86 and B3LYP functionals assign similar spin densities to iron and oxygen and so do not return fundamentally different bonding electronic structures. Instead, it appears that the functionals struggle to assign the correct energy because of these nondynamic correlation effects. It has

dx.doi.org/10.1021/ic500379r | Inorg. Chem. 2014, 53, 6473−6481

been suggested that such correlation effects are described in a nonsystematic way in DFT, leading to systematic errors in relative energies that are particularly strong in transition-metal compounds.[44] As is often the case where nondynamic correlation effects are poorly treated by DFT, changing the amount of exact exchange in the DFT functional strongly changes the calculated energies. This is shown here by the difference between the B3LYP (20% exact exchange) and BP86 (0%) results. In the SI, we show that related changes in the relative energies are obtained upon a change in the amount of exact exchange in the B3LYP functional. Benchmark CCSD-(T)-F12 calculations, which appear to describe the correlation effects in this system reasonably well, enable us to conclude that the B3LYP functional is closer to being accurate than BP86 for this system. This suggests that the B3LYP calculations agree with experiment because they provide an accurate model of the Fenton reaction.

The present study also analyzes in some detail the factors that affect the accuracy of the DFT calculations. These include, beyond the choice of functional, the basis set (chosen to be fairly large here), relativity, and solvation. The last two change the relative energies by many kilocalories per mole. Another important aspect is the accurate location of minima on the potential energy surface, which proved difficult in the present case because these minima nearly correspond to quite highly symmetric structures. Because of the presence of imaginary frequencies in the symmetrized structures, free-energy analyses obtained from these are not accurate, and we were careful to instead use correct minima.

The calculated rate constant for the reaction of H_2O_2 with iron(II) and the calculated pK_a values for the iron(II) and iron(IV) systems are incorrect by factors consistent with errors in free energies by 4 kcal mol^{-1}. This suggests that obtaining accurate free energies for aqueous transition-metal-ion chemistry remains challenging and that mechanistic conclusions based on computational studies of such systems should be appropriately cautious. The newly developed correlation methods with explicit correlation (CCSD(T)-F12[27]) do provide some progress in this respect because they enable correlated energies to be obtained at effectively the basis set limit, even for midsized metal complexes (15−30 atoms) such as those studied here. Also, continuum solvent methods provide accurate estimates of free energies in solution,[29] and these combined developments do mean that our calculated free energies here are much more accurate than would have been available some time ago. We estimate that the free energies here are accurate to within ca. 5 kcal mol^{-1}.

■ ASSOCIATED CONTENT

Supporting Information

Effect of exact exchange and detailed computational results. This material is available free of charge via the Internet at http://pubs.acs.org.

■ AUTHOR INFORMATION

Corresponding Author

*E-mail: jeremy.harvey@bristol.ac.uk.

Notes

The authors declare no competing financial interest.

■ ACKNOWLEDGMENTS

We acknowledge EPSRC for a Ph.D. studentship (to R.C.R.P.).

■ REFERENCES

(1) For example, see: Armentrout, P. B.; Halle, L. F.; Beauchamp, J. L. *J. Am. Chem. Soc.* **1981**, *103*, 6501−6502.
(2) Fiedler, A.; Schröder, D.; Shaik, S.; Schwarz, H. *J. Am. Chem. Soc.* **1994**, *116*, 10734−10741.
(3) Carter, E. A.; Goddard, W. A. *J. Phys. Chem.* **1988**, *92*, 2109−2115.
(4) Dietl, N.; van der Linde, C.; Schlangen, M.; Beyer, M. K.; Schwarz, H. *Angew. Chem., Int. Ed.* **2011**, *50*, 4966−4969.
(5) Schröder, D.; Schwarz, H.; Clemmer, D. E.; Chen, Y. M.; Armentrout, P. B.; Baranov, V. I.; Bohme, D. K. *Int. J. Mass Spectrom. Ion Processes* **1997**, *161*, 175−191.
(6) Harvey, J. N.; Tew, D. P. *Int. J. Mass Spectrom.* **2013**, *354*−*355*, 263−270.
(7) Schröder, D.; Schwarz, H. *Angew. Chem., Int. Ed. Engl.* **1990**, *29*, 1431−1433.
(8) Winkler, J. R.; Gray, H. B. *Struct. Bonding (Berlin)* **2012**, *142*, 17−28.
(9) Rohde, J. U.; In, J. H.; Lim, M. H.; Brennessel, W. W.; Bukowski, M. R.; Stubna, A.; Münck, E.; Nam, W.; Que, L. *Science* **2003**, *299*, 1037−1039. Nam, W. *Acc. Chem. Res.* **2007**, *40*, 522−531.
(10) Krebs, C.; Fujimori, D. G.; Walsh, C. T.; Bollinger, J. M. *Acc. Chem. Res.* **2007**, *40*, 484−492.
(11) Usharani, D.; Janardanan, D.; Li, C. S.; Shaik, S. *Acc. Chem. Res.* **2013**, *46*, 471−482.
(12) Blomberg, M. R. A.; Borowski, T.; Himo, F.; Liao, R. Z.; Siegbahn, P. E. M. *Chem. Rev.* **2014**, *114*, 3601−3658.
(13) McDonald, M. R.; Que, L. *Coord. Chem. Rev.* **2012**, *257*, 414−428.
(14) Shaik, S.; Cohen, S.; Wang, Y.; Chen, H.; Kumar, D.; Thiel, W. *Chem. Rev.* **2010**, *110*, 949−1017.
(15) Schoneboom, J. C.; Lin, H.; Reuter, N.; Thiel, W.; Cohen, S.; Ogliaro, F.; Shaik, S. *J. Am. Chem. Soc.* **2002**, *124*, 8142−8151.
(16) Rittle, J.; Green, M. T. *Science* **2010**, *330*, 933−937.
(17) For experimental work in this area, see, e.g.: Kanan, M. W.; Nocera, D. G. *Science* **2008**, *321*, 1072−1075.
(18) For computational studies, see, e.g.: Wang, L.-P.; Wu, Q.; Van Voorhis, T. *Inorg. Chem.* **2010**, *49*, 4543−4553.
(19) Dunford, H. B. *Coord. Chem. Rev.* **2002**, *233/234*, 311−318.
(20) Pestovsky, O.; Stoian, S.; Bominaar, E. L.; Shan, X.; Münck, E.; Que, L., Jr.; Bakac, A. *Angew. Chem., Int. Ed.* **2005**, *44*, 6871−6874.
(21) Bataineh, H.; Pestovsky, O.; Bakac, A. *Chem. Sci.* **2012**, *3*, 1594−1599.
(22) Ensing, B.; Buda, F.; Blöchl, P.; Barends, E. J. *Angew. Chem., Int. Ed.* **2001**, *40*, 2893−2895. Buda, F.; Ensing, B.; Gribnau, M. C. M.; Baerends, E. J. *Chem.—Eur. J.* **2001**, *7*, 2775−2783. Ensing, B.; Baerends, E. J. *J. Phys. Chem. A* **2002**, *106*, 7902−7910.
(23) Yamamoto, N.; Koga, N.; Nagaoka, M. *J. Phys. Chem. B* **2012**, *116*, 14178−14182.
(24) Tan, E. H. P.; Lloyd-Jones, G. C.; Harvey, J. N.; Lennox, A. J. J.; Mills, B. M. *Angew. Chem., Int. Ed.* **2011**, *50*, 9602−9606.
(25) Cramer, C. J.; Truhlar, D. G. *Phys. Chem. Chem. Phys.* **2009**, *11*, 10757−10816.
(26) Cramer, C. *Essentials of Computational Chemistry*, 2nd ed.; John Wiley and Sons: Chichester, U.K., 2004.
(27) Cooper, J.; Ziegler, T. *Inorg. Chem.* **2002**, *41*, 6614−6622. Lau, J. K.-C.; Deubel, D. V. *J. Chem. Theory Comput.* **2006**, *2*, 103−106.
(28) Harvey, J. N. *Faraday Discuss.* **2010**, *145*, 487−505.
(29) Adler, T. B.; Knizia, G.; Werner, H.-J. *J. Chem. Phys.* **2007**, *127*, 221106. Adler, T. B.; Knizia, G.; Werner, H.-J. *J. Chem. Phys.* **2009**, *130*, 054104.
(30) Grimme, S. *J. Comput. Chem.* **2006**, *27*, 1787−1799.
(31) Fouqueau, A.; Mer, S.; Casida, M. E.; Lawson Daku, L. M.; Hauser, A.; Mineva, T.; Neese, D. *J. Chem. Phys.* **2004**, *120*, 9473−9486.
(32) Deeth, R. J.; Anastasi, A. E.; Randell, K. *Dalton Trans.* **2009**, 6007−6012.
(33) Marenich, A. V.; Cramer, C. J.; Truhlar, D. G. *J. Phys. Chem. B* **2009**, *113*, 6378−6396.

(34) Frisch, M. J.; Trucks, G. W.; Schlegel, H. B.; Scuseria, G. E.; Robb, M. A.; Cheeseman, J. R.; Scalmani, G.; Barone, V.; Mennucci, B.; Petersson, G. A.; Nakatsuji, H.; Caricato, M.; Li, X.; Hratchian, H. P.; Izmaylov, A. F.; Bloino, J.; Zheng, G.; Sonnenberg, J. L.; Hada, M.; Ehara, M.; Toyota, K.; Fukuda, R.; Hasegawa, J.; Ishida, M.; Nakajima, T.; Honda, Y.; Kitao, O.; Nakai, H.; Vreven, T.; Montgomery, J. L., Jr.; Peralta, J. E.; Ogliaro, F.; Bearpark, M.; Heyd, J. J.; Brothers, E.; Kudin, K. N.; Staroverov, V. N.; Keith, T.; Kobayashi, R.; Normand, J.; Raghavachari, K.; Rendell, A.; Burant, J. C.; Iyengar, S. S.; Tomasi, J.; Cossi, M.; Rega, N.; Millam, J. M.; Klene, M.; Knox, J. E.; Cross, J. B.; Bakken, V.; Adamo, C.; Jaramillo, J.; Gomperts, R.; Stratmann, R. E.; Yazyev, O.; Austin, A. J.; Cammi, R.; Pomelli, C.; Ochterski, J. W.; Martin, R. L.; Morokuma, K.; Zakrzewski, V. G.; Voth, G. A.; Salvador, P.; Dannenberg, J. J.; Dapprich, S.; Daniels, A. D.; Farkas, O.; Foresman, J. B.; Ortiz, J. V.; Cioslowski, J.; Fox, D. J. *Gaussian 09*, revision B.01; Gaussian, Inc.: Wallingford, CT, 2010.

(35) Werner, H.-J.; Knowles, P. J.; Knizia, G.; Manby, F. R.; Schütz, M.; Celani, P.; Korona, T.; Lindh, R.; Mitrushenkov, A.; Rauhut, G.; Shamasundar, K. R.; Adler, T. B.; Amos, R. D.; Bernhardsson, A.; Berning, A.; Cooper, D. L.; Deegan, M. J. O.; Dobbyn, A. J.; Eckert, F.; Goll, E.; Hampel, C.; Hesselmann, A.; Hetzer, G.; Hrenar, T.; Jansen, G.; Köppl, C.; Liu, Y.; Lloyd, A. W.; Mata, R. A.; May, A. J.; McNicholas, S. J.; Meyer, W.; Mura, M. E.; Nicklass, A.; O'Neill, D. P.; Palmieri, P.; Pflüger, K.; Pitzer, R.; Reiher, M.; Shiozaki, T.; Stoll, H.; Stone, A. J.; Tarroni, R.; Thorsteinsson, T.; Wang, M.; Wolf, A. *MOLPRO*, version 2010.1, a package of ab initio programs; see http://www.molpro.net.

(36) Balabanov, N. B.; Peterson, K. A. *J. Chem. Phys.* **2005**, *123*, 064107.

(37) Dunand, F. A.; Helm, L.; Merbach, A. E. *Coord. Chem. Rev.* **2003**, *54*, 1−69.

(38) Novikov, A. S.; Kuznetsov, M. L.; Pombeiro, A. J. L.; Bokach, N. A.; Shul'pin, G. B. *ACS Catal.* **2013**, *3*, 1195−1208.

(39) Grimme, S. *WIREs Comput. Mol. Sci.* **2011**, *1*, 211−228.

(40) Harvey, J. N. *J. Biol. Inorg. Chem.* **2011**, *16*, 831−839.

(41) Pyykko, P. *Chem. Rev.* **1988**, *88*, 563−594.

(42) Isse, A. A.; Gennaro, A. *J. Phys. Chem. B* **2010**, *114*, 7894−7899.

(43) Ho, J.; Coote, M. L. *Theor. Chem. Acc.* **2010**, *125*, 3−21.

(44) Friesner, R. A.; Knoll, E. H.; Cao, Y. *J. Chem. Phys.* **2006**, *125*, 124107. Hughes, T. F.; Friesner, R. A. *J. Chem. Theory Comput.* **2011**, *7*, 19−32. Hughes, T. F.; Harvey, J. N.; Friesner, R. A. *Phys. Chem. Chem. Phys.* **2012**, *14*, 7724−7738.

dx.doi.org/10.1021/ic500379r | *Inorg. Chem.* 2014, 53, 6473−6481